

Scaling law for viscous friction in thin lubricating films that acts on a solid disk falling in confined space

Nana Tanaka and Ko Okumura

Physics Department and Soft Matter Center, Ochanomizu University, Japan

(Dated: April 24, 2022)

Abstract

We fill a viscous liquid in a vertically stood cell of millimeter thickness, called the Hele-Shaw cell, and insert a disk in the liquid whose thickness is smaller than the cell thickness. The disk starts falling in the liquid due to gravity with opposed by viscous friction. We focus on the case in which lubricating films formed in the gap between the cell surface and the disk surface are thinner than the disk thickness. As a result, we find a distinct regime in which the flow and the viscous friction are characterized by the thickness of the lubricating film. The scaling regime is identified through clear collapse of the data onto a master curve. We also discuss the case in which lubricating films are thick. The present results are relevant to fundamental issues and applications in various fields such as microfluidics, bioconvection, and active matter.

I. INTRODUCTION

A classic problem of viscous friction acting on an object receives growing attention in various contexts. In microfluidics [1], promising for applications in chemistry, biology, medicine and pharmaceutical industry, viscous friction manifests as important in various geometries, due to the confinement of liquid. Bioconvection, resulting from swimming of a large number of small objects, has been studied in biology and has recently been received considerable attention in active matter [2–4]. The central issue of this problem is flow at low Reynolds numbers governed by viscous friction.

Relevant classic studies are motion of a bubble in a capillary tube [5] and in a Hele-Shaw cell [6]. Our focus in the present study is on the latter. A number of studies have been performed in the Hele-Shaw geometry. However, until recently, the existence of lubricating film between the cell surface and bubble surface have not been highlighted, and related studies have been studied mainly with a forced flow and/or with nearly horizontal geometries [7–10].

We have recently focused on the lubricating film, using a vertically stood Hele-Shaw cell of millimeter thickness, filled with viscous liquid. As a result, we have established a number of scaling regimes for drag friction acting on fluids surrounded by another immiscible fluid [11–14]. Furthermore, other groups have explored closely related issues, using cells with smaller scales [15, 16] and comparing numerical results with experiment [17].

In this study, we explore a seemingly simpler case of drag friction acting on a solid disk in a Hele-Shaw cell of millimeter thickness, where similar lubricating films exist between the cell wall and disk surface. Our principal interest is in the case in which the thickness of the lubrication film is smaller than the disk thickness when the disk falling in the direction perpendicular to its axis. As far as we know, this case has not been explored in the literature, while it is closely related a study of transport of strongly confined disks under flow in microfluidic devices [18]. As a result, we identified a clear scaling regime, which can be interpreted based on physical arguments. We also discuss the limitation of this scaling regime.

The present experiment is an extreme case of a Stokes drag friction F for a solid disk moving in a direction perpendicular to the axis, i.e., in a direction of the disk plane. For later convenience, we briefly review relevant previous studies starting from a non-confined

case. In this context, there are two important geometrical parameters. One is the ratio of the radius of the disk R to the distance of the cell plates parallel to the disk plane D , or a measure of confinement:

$$C = R/D. \quad (1)$$

The other is the thickness D_0 to radius R , or the aspect ratio of the disk:

$$A = D_0/R \quad (2)$$

An early study by Oberbeck on the issue in 1876 gave a Stokes drag friction F_O under no confinement ($C = 0$) for a disk of zero thickness ($A = 0$):

$$F_O = 32\eta VR/3 \quad (3)$$

with η the viscosity of surrounding liquid and V the velocity of the disk [19]. In 1962, Brenner considered the effect of a weak confinement, i.e., $C \ll 1$, for the zero thickness ($A = 0$), to give a first-order correction to the drag coefficient

$$K = F/F_O \quad (4)$$

in the expansion in terms of C [20] (note that $K \geq 1$ due to confinement). In 1991, Davis developed analytical theory for stronger confinement in the case of zero thickness ($A = 0$) (see Sec. 4 of [21]), and numerically presented the value of the drag coefficient K up to a large value ($C = 4$), based on the analytical expression. In 1984 and 1999, Roger et al. theoretically considered when the disk thickness is finite [22] but under no confinement ($C = 0$), and compared experimental results for finite thickness. In 2006, Trahan conducted experiments using disks of finite thickness under weak confinement for very thin disks, to give an empirical fitting formula, which gives the coefficient K as a function of A and C [23]. Although the fitting function well captures their data, the function contains six fitting parameters and the physical origin of the complex form of the function was not justified. It is stressed here that in the literature there are no analytical expressions based on physical justification when both A and C are finite. In fact, Trahan's principle aim was to experimentally justify Davis' result [21], which is the case of $A = 0$. In addition, Trahan

did not deal with the case the thickness of lubricant film h defined below is smaller than the disk thickness D_0 , which is the main focus of the present study.

II. EXPERIMENT

We filled a Hele-Shaw cell, stood vertically, with a silicone oil (polydimethylsiloxane, PDMS) as shown in Fig. 1 (a). We inserted a metal disk of radius $R = 10$ mm at the top of the cell with a zero initial speed. We recorded the ensuing falling motion of the metal with a camera after the disk began going down in the cell at a constant speed. As indicated in the side view (Fig. 1 (a)), we expect two lubricating films of thickness h are formed between the cell inner surface and the disk surface (see the details below).

The width and height of the cell was 90 and 160 mm, respectively. We checked the thickness D of the cell using a laser censer (ZS-HLDS5, Omron) and its controller (ZS-HLDC11, Omron) to find D was in the range of 2.2 to 7 mm (we also provided the data for larger D to show the breakdown of the regime of our principal interest). The viscosity η of PDMS was in the range of 0.490 to 9.57 Pa·s. This corresponds to the range of the kinematic viscosity ν , 1000 to 10000 cS. The metal disk is a stainless-steel 403 of density 7.70 g/cm³, which can be manipulated by a magnet placed on the cell surface. The thickness D_0 ($< D$) of the disk was either 0.952, 1.88, 2.87, or 3.90 mm (these three thicknesses will be labeled as $D_0 = 1, 2, 3$, and 4 mm, for convenience, in the following). We used a digital camera (EX-F1, Casio) setting the time interval in the range of 1 to 1/60 second. The digital images were analyzed with a software, Image J.

III. RESULTS

A. Falling motion

As demonstrated in Fig. 1 (b), the velocity of falling motion of the disk reached a constant speed, which was reasonably reproducible at a given experimental parameter set, η , D_0 , and h with $2h = D - D_0$. Here, h is the thickness of two viscous liquid films, each of which is sandwiched by an inner surface of cell plate and a surface of the disk. To obtain reproducible data, we need to satisfy the condition $2h = D - D_0$ at the entry: the disk should be vertical and the disk center should match the that of the cell (in the thickness direction).

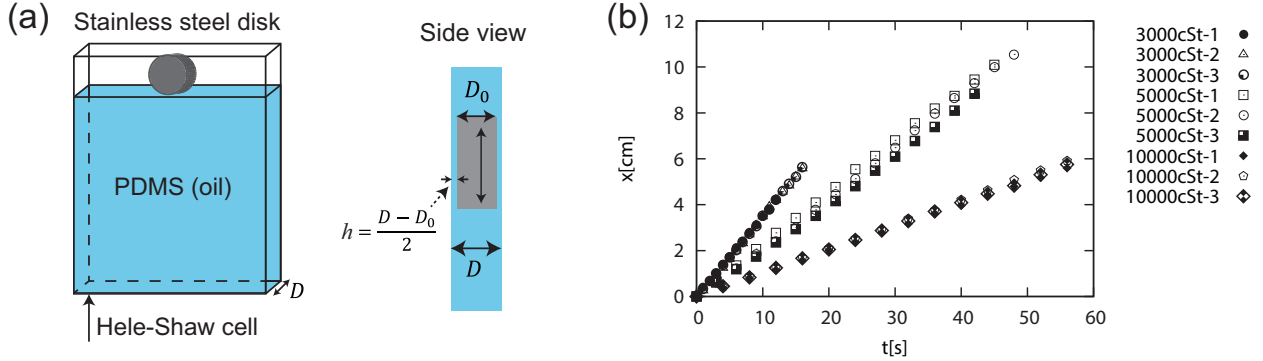


FIG. 1: (a) Illustration of experiment. A metal disk of thickness D_0 is dropped in the cell of width D filled with a viscous oil of kinematic viscosity ν . The side view suggests the existence of two lubricating films of thickness h . (b) Vertical position x vs time t . Results of three falling experiments are shown for each parameter set: ν , D , and D_0 . The data labeled 3000, 5000, and 10000 cS are performed for $(\nu, D, D_0) = (3000, 2.61, 1.88)$, $(5000, 2.59, 1.88)$ and $(10000, 2.52, 1.88)$, respectively, with D and D_0 given in mm.

Experiments were performed carefully to satisfy these entry condition. For this purpose, it was helpful to set a gate of width comparable to the disk thickness D_0 at the entry point and to keep in mind that the falling speed should be maximized when the condition is well satisfied. As a result, errors for velocity were typically less than 10 per cent.

B. The falling velocity at different parameters

In Fig. 2 (a)-(c), we present the falling velocity V , obtained as a slope in the $x - t$ plot as in Fig. 1 (b), as a function of the film thickness h for $h < D_0$. Details of the data presentation are as follows. One data point, without error bars, corresponds to each falling experiment. We repeated falling experiments typically several times (in the range twice to more than 10 times) for a single parameter set and we showed all the results in the plots. As a result, in some case data points are closely overlapped, which suggests a size of errors in the measurements.

In Fig. 2 (a)-(c), we observe a coherent and systematic parameter dependence: V increases with h and D_0 but decreases with η , showing viscous origin of the dynamics. Note that differences in color and mark correspond to those in D_0 and η , respectively.

In Fig. 2 (d), we explore a wider range of h for $\eta = 3000$ cS to see the limitation of the regime of our principal interest. Here, we use the same color convention, but assign different marks as specified in the caption.

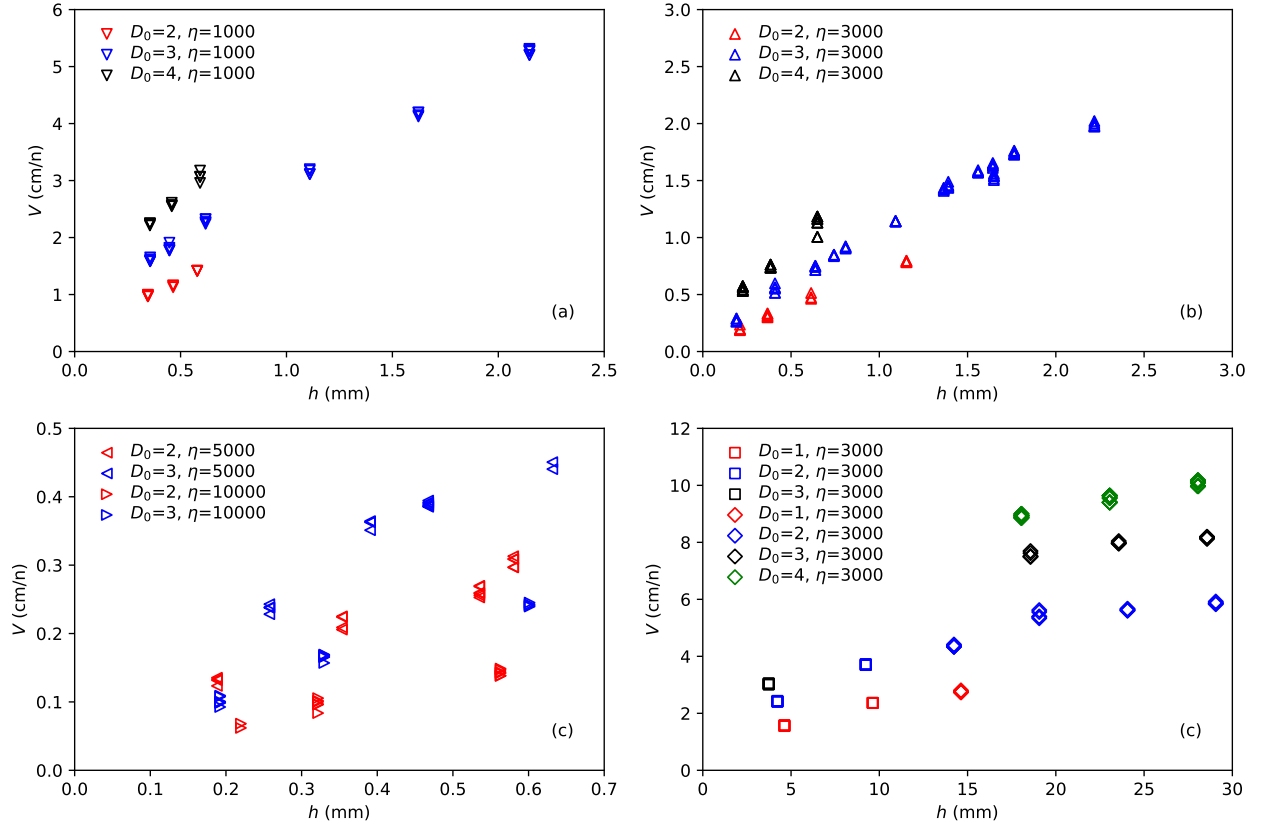


FIG. 2: (a)-(c): V vs h for $h < D_0$. (a) $\eta = 1000$ cS. (b) $\eta = 3000$ cS. (c) $\eta = 5000$ and 10000 cS. (d) V vs h at $\eta = 3000$ cS for $h > D_0$. Colors and marks differentiate D_0 and η , respectively. When $h > D_0$ (only for $\eta = 3000$ cS), we assigned different marks. Open squares and diamonds correspond to the data satisfying $D_0 < h < R$ and $h > R$, respectively (note that $R > D_0$). The labels for D_0 and η are given in mm and cS (as for D_0 , the corresponding precise values are given in the text).

C. Dimensional analysis

The viscosity dependence of the velocity indicates that the dynamics is governed by gravity opposed by viscosity. The gravitational energy gain per time is trivially given as $\sim \Delta\rho g R^2 D_0 V$, corresponding to a gravitational force, $\Delta\rho g R^2 D_0$. As for the viscous dissipation, we here consider the extreme case of $h \ll R$. In this limit, the viscous dissipation may be characterized by the smallest length scale h of the problem: the dissipation in the unit volume per time scales as $\eta(V/h)^2$. This occurs inside the two viscous liquid films, each covering the disk surface of area $\sim R^2$. The total dissipation per time amounts to $\eta(V/h)^2 R^2 h$. Balance of the gravitational energy gain with this dissipation gives

$$V \sim \Delta\rho g D_0 h / \eta \quad (5)$$

This corresponds to the following viscous drag and the drag coefficient:

$$F \sim \eta(V/h)R^2 \quad (6)$$

$$K \sim R/h \quad (7)$$

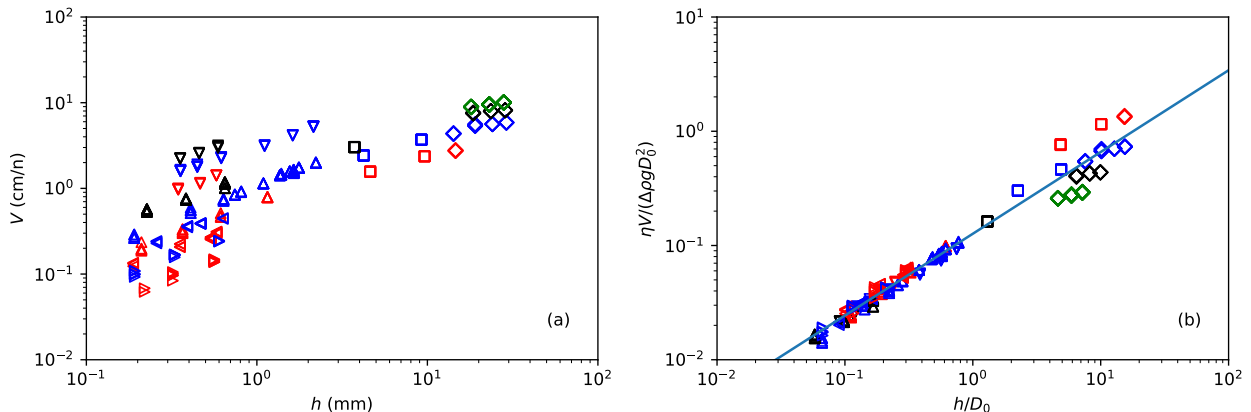


FIG. 3: (a) V vs h on a log-log scale. All the data in Fig. 2 are shown. (b) Renormalized version of (a), which confirms the first regime is governed by Eq. (5).

D. Agreement between experiment and theory

In Fig. 3 (a), we collect all the data in Fig. 2 on a single plot on a log-log scale. The total number of the data points shown in Fig. 3 (a) are 367 and they are obtained for 74 different parameter set (D_0, η, h) .

In Fig. 3 (b) we plot the renormalized velocity $\eta V/(\Delta\rho g D_0^2)$ as a function of the renormalized thickness h/D_0 , using all the data in Fig. 3 (a): since Eq. (5) can be expressed as $\eta V/(\Delta\rho g D_0^2) \sim h/D_0$, the data described by Eq. (5) should collapse onto a master curve on this plot. This is what we observe in Fig. 3 (b): the data for $h < D_0$ (all the data except for open squares and diamonds), which well satisfy $h \ll R$ (note $D_0 \ll R$), collapse well on the master curve.

However, the agreement is not perfect. As a result of numerical fitting, we find that the collapsed data, i.e., all the data in Fig. 3 except for open squares and diamonds, are well described by the following expression

$$\eta V/(\Delta\rho g D_0^2) = k_1(h/D_0)^\alpha \quad (8)$$

with $k_1 = 0.127 \pm 0.001$ and $\alpha = 0.716 \pm 0.008$. Note that the exponent α deviates from the theoretical prediction $\alpha = 1$.

IV. DISCUSSION

A. Slight deviation from the prediction

The reason α is slightly less than unity in Eq. (8) should be explored in the future. In the light of Eq. (5), V should linearly approach zero as h decreases: scaling arguments predict $\alpha = 1$. However, all the data in Fig. 2 (a)-(c) are well described by Eq. (8) with α slightly less than unity. In fact, the data of the same color in Fig. 2 (b) and (c) do not seem on the straight line, but rather seem to smoothly go to the origin $(h, V) = (0, 0)$ by extrapolation, which is consistent with the fitting with α slightly less than unity.

The data in Fig. 2 (a) may seem to be on the straight line, but may also seem to smoothly go to the origin by extrapolation. However, the latter view is supported by the overall fitting. In addition, the former view implies the slip length of the order of 0.1 mm (note that the simple linear extrapolation of the data of each color in Fig. 2 (a) may intersect the horizontal axis at a value around $h = -0.1$ to -0.3 mm). This order of magnitude is too large for the slip length. This characteristic length has been discussed for polymer liquids [24] and its typical order estimated by the reptation model [24, 25] is monomer scale multiplied by the ratio of melt viscosity to monomer viscosity. This suggests that, in the present case, the slip length may at most $10\mu\text{m}$. This means that the present experiment is not appropriate to discuss the slip length. For this purpose, we need to explore the case in which h is even smaller, which is technically challenging.

B. Data for $h > D_0$

In Fig. 2 (d), we provided the data for $h > D_0$ and showed these data do not collapse well on the master curve, on which the data for $h < D_0$ collapse well. In this case of $h > D_0$, Trahan [23] provided the data in the range $0.025 < A/2 = D_0/2R < 0.0759$ and $0.1623 < 2C = 2R/D < 3.890$ (as seen in Fig. 4 (a), compared with the present case, the aspect ratio A in [23] is generally much smaller). Trahan showed that the data are

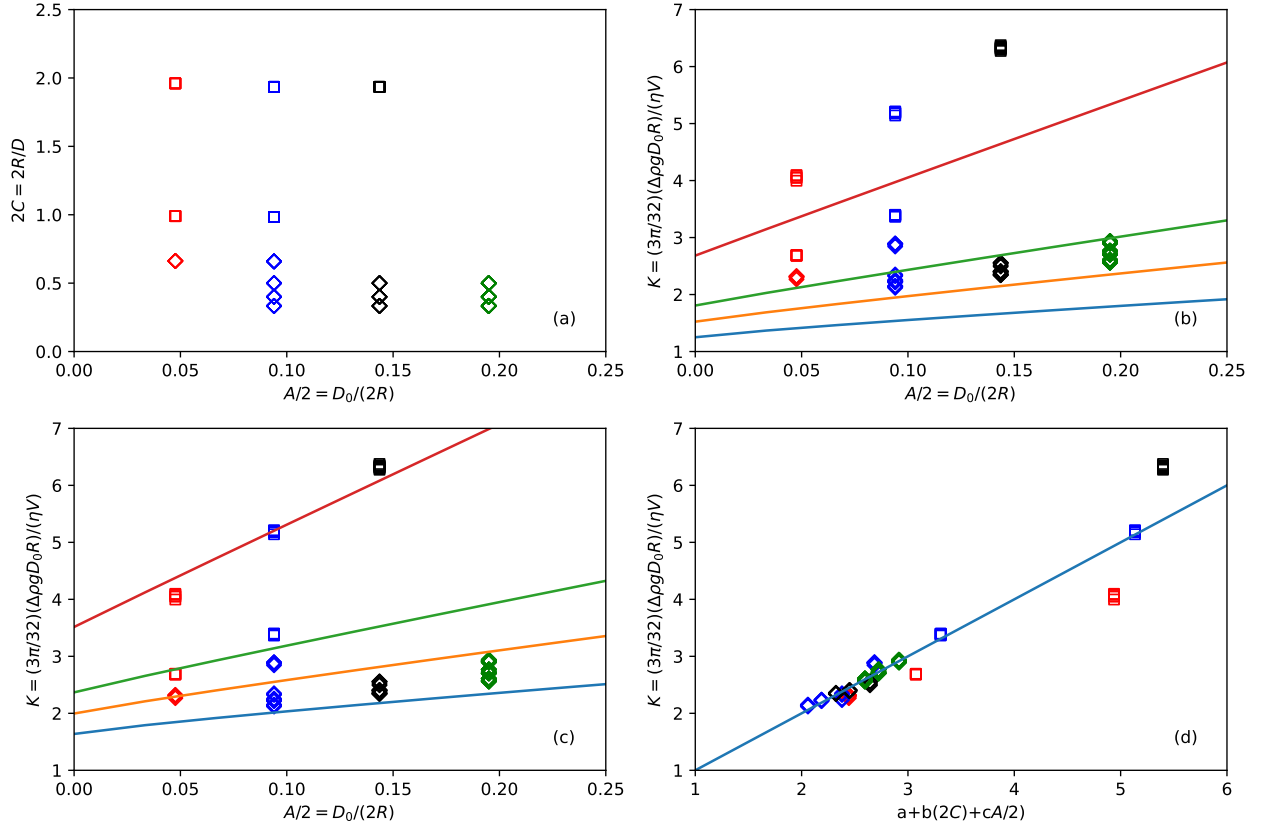


FIG. 4: (a) Range of the aspect ratio $A/2 = D_0/(2R)$ and the confinement parameter $2C = 2R/D$ of the present study for $h > D_0$. (b) The drag coefficient K as a function of $A/2 = D_0/(2R)$. Solid lines show Eq. (9) for four different values of $2C = 2R/D$ (see the text for the details). (c) The same plot with (b) but with a factor 1.31 multiplied for solid lines. (d) K obtained from velocity vs fit based on Eq. (10).

quantitatively well described by the following expression containing six fitting parameters:

$$K = 1 + a(2C)^b + (f + g(2C))^2(A/2)^{1-k} \exp(-p(2C)) \quad (9)$$

with $a = 0.8160$, $b = 1.0754$, $f = 1.0418$, $g = 1.3312$, $k = 0.2269$, and $p = 1.51$. This complex form was proposed only on the basis that a fit in a much simpler form of $K = b'(A/2)^{c'}$ with b' and c' constants worked well in the case of $C = 0$.

As explained below, we can confirm the expression in Eq. (9) is valid only qualitatively for the present data for $h > D_0$: K increases with $A/2$ and the increase becomes significant as $2C$ increases.

In Fig. 4 (b), we draw four straight lines, which represents Eq. (9) for four values of $2C$ to compare them with the present data: $2C = 20/60 \simeq 0.33$, $20/30.3 \simeq 0.66$, $20/20.2$

$\simeq 0.99$, and $20/10.2 \simeq 1.96$. The lower and highest straight lines correspond to $2C = 20/60$ and $10/10.2$, respectively. Note here that K in the present case can be obtained from the measured velocity V using the relation $(32/3)\eta V R K = \Delta\rho g \pi R^2 D_0$.

In Fig. 4 (b), if Eq. (9) describes well the present data, all the open squares above the highest straight line should be on this line, which is not the case. In addition, if Eq. (9) is valid, the lowest open diamonds of each color should be on the lowest straight line, which is also not the case. In other words, Eq. (9) fails to describe the present data in a quantitative manner.

As mentioned above, in general, Trahan investigated cases of smaller A than in the present study. Accordingly, only the red diamonds at $(A/2, 2C) = (0.952/20, 20/30.2) \simeq (0.048, 0.66)$ and the red squares at $(A/2, 2C) = (0.952/20, 20/20.2) \simeq (0.048, 0.99)$ in Fig. 4 (a) are in the overlapping region. In Fig. 4 (b), these two sets of data are red squares and diamonds in between the highest and second highest straight lines, and they should be on the second and third highest straight lines, respectively, if Eq. (9) is valid, which is not the case.

Even though if we determine a factor for Eq. (9) so that the line representing Eq. (9) with the factor goes through red diamonds and replot the four straight lines with the same factor, qualitative agreement was not obtained, as seen in Fig. 4 (c).

To physically understand the present data with $h > D_0$, we consider three dissipations: $\eta(V/R)^2 R^3$, $\eta(V/D)^2 R^2 D$, and $\eta(V/R)^2 R^2 D_0$ per unit time (note that the first term corresponds to the Oberbeck case). When the sum of the three dissipation with factors (a, b , and c) is balanced with the gravitational energy gain $\Delta\rho g R^2 D_0 V$, we obtain a physically motivated form:

$$K = a + b(2C) + c(A/2) \quad (10)$$

With this function, we fit the data marked with diamonds, which are the data satisfying the conditions $h < D_0$ and both $2C = 2R/D$ and $A/2 = D_0/(2R)$ smaller than one (we expect that Eq. (10) should be valid for small C and A in the light of previous studies such as [20] and [22]). The result of fitting is shown in Fig. 4 (c) where $a = 0.920 \pm 0.063$, $b = 3.84 \pm 0.19$, and $c = 5.31 \pm 0.20$. All the diamonds are reasonably well represented by the fitting line, which supports Eq. (10). (Trahan proposed an expression $K = 1 + 0.8160(2C)^{1.0754}$ in the case of $A = 0$, which is close to Eq. (10) with $a = 1$ and $b = 0.8160$. Compared with this,

the value we obtained for b (3.84) is larger, which may be because we are dealing with the case of finite A).

C. Difference from the case of fluid "disk" falling in confined viscous liquid

The scaling regime governed by Eq. (5) proposed in the present study is inherently different from the case in which the disk is replaced with a fluid "disk." The latter case is studied in our previous study [12], in which, the thickness of lubricating film h and the disk thickness (or, the shape of fluid drop) are dynamically determined, with the former governed by the law of Landau, Levich, and Derjaguin (LLD) [26, 27]. As a result, h depends on the falling velocity V , which leads to an unusual nonlinear drag force F . The drag force in the fluid case scales with $V^{1/3}$. In the present case, h is fixed by the (fixed) disk thickness, which leads to a usual linear drag force F scaling simply with V .

In microfluidic applications, fluid drops of various kind have been utilized, which include armored bubbles or drops, gelified drops, bubbles and drops with rigid and mobile surfactants. Such cases could be similar to the bubble case compared with the solid case in that the lubricating film thickness is dynamically determined. However, the detailed boundary condition could be more delicate compared with the two limiting cases of a simple bubble or a solid disk and thus worth studying in the future. Note that even if the thickness of the lubricating film is determined dynamically, the dissipation in the film can be irrelevant to the drag force as shown in [11].

V. CONCLUSION

In the present study, we investigated the falling velocity of a solid disk in viscous liquid in a confined space and the drag friction acting on the disk. We successfully identified a scaling regime, proposing scaling laws for the velocity and drag friction. Although the data collapsed well, the scaling exponent α is slightly smaller than the predicted value $\alpha = 1$. To resolve this issue, we may need to perform a separate study. In the Discussion, we also examine the data we obtained for weakly confined case and provide detailed comparison with previous study.

Fundamental understandings on fluid flow at low Reynolds numbers provided in the

present study should be valid for small objects in less viscous liquid such as water. Accordingly, the present results are relevant to various fundamental issues and applications, for example, in microfluidics, bioconvection and active matter, in which viscous friction acting on small objects are highly important.

Conflicts of interest

There are no conflicts of interest to declare.

Acknowledgments

This work was partly supported by JSPS KAKENHI Grant Number JP19H01859.

-
- [1] Squires, T. M. & Quake, S. R. Microfluidics: Fluid physics at the nanoliter scale. *Rev. Mod. Phys.* **77**, 977 (2005).
 - [2] Bees, M. A. Advances in bioconvection. *Annual Review of Fluid Mechanics* **52**, 449–476 (2020).
 - [3] Kage, A., Hosoya, C., Baba, S. A. & Mogami, Y. Drastic reorganization of the bioconvection pattern of chlamydomonas: quantitative analysis of the pattern transition response. *Journal of Experimental Biology* **216**, 4557–4566 (2013).
 - [4] Ramaswamy, S. The mechanics and statistics of active matter. *Annu. Rev. Condens. Matter Phys.* **1**, 323–345 (2010).
 - [5] Bretherton, F. P. The motion of long bubbles in tubes. *J. Fluid. Mech.* **10**, 166 (1961).
 - [6] Saffman, P. G. & Taylor, G. The penetration of a fluid into a porous medium or hele-shaw cell containing a more viscous liquid. *Proc. R. Soc. London, Ser. A* **245**, 312–329 (1958).
 - [7] Tanveer, S. The effect of surface tension on the shape of a hele–shaw cell bubble. *Phys. Fluids* **29**, 3537–3548 (1986).
 - [8] Maxworthy, T. Bubble formation, motion and interaction in a hele-shaw cell. *J. Fluid Mech.* **173**, 95–114 (1986).

- [9] Kopf-Sill, A. R. & Homsy, G. M. Bubble motion in a hele–shaw cell. *Phys. Fluids* **31**, 18–26 (1988).
- [10] Maruvada, S. R. K. & Park, C.-W. Retarded motion of bubbles in hele–shaw cells. *Phys. Fluids* **8**, 3229–3233 (1996).
- [11] Eri, A. & Okumura, K. Viscous drag friction acting on a fluid drop confined in between two plates confined in between two plates. *Soft Matter* **7**, 5648 (2011).
- [12] Yahashi, M., Kimoto, N. & Okumura, K. Scaling crossover in thin-film drag dynamics of fluid drops in the hele-shaw cell. *Sci. Rep.* **6**, 31395 (2016).
- [13] Okumura, K. Viscous dynamics of drops and bubbles in hele-shaw cells: drainage, drag friction, coalescence, and bursting. *Advances in Colloid and Interface Science*; <https://doi.org/10.1016/j.cis.2017.07.021> (2017).
- [14] Murano, M. & Okumura, K. Rising bubble in a cell with a high aspect ratio cross-section filled with a viscous fluid and its connection to viscous fingering. *Physical Review Research* **2**, 013188 (2020).
- [15] Keiser, L., Jaafar, K., Bico, J. & Reyssat, É. Dynamics of non-wetting drops confined in a hele-shaw cell. *Journal of Fluid Mechanics* **845**, 245–262 (2018).
- [16] Keiser, L., Keiser, A., Lestimé, M., Bico, J. & Reyssat, E. Motion of viscous droplets in rough confinement: paradoxical lubrication. *Physical review letters* **122**, 074501 (2019).
- [17] Shukla, I., Kofman, N., Balestra, G., Zhu, L. & Gallaire, F. Film thickness distribution in gravity-driven pancake-shaped droplets rising in a hele-shaw cell. *J. Fluid. Mech* **874**, 1021 (2019).
- [18] Uspal, W. E., Eral, H. B. & Doyle, P. S. Engineering particle trajectories in microfluidic flows using particle shape. *Nature communications* **4**, 1–9 (2013).
- [19] Oberbeck, A. Ueber stationaere fluessigkeitsbewegungen mit beruecksichtigung der inneren reibung. *J. Reine Angew. Math.* **81**, 62–80 (1876).
- [20] Brenner, H. Effect of finite boundaries on the stokes resistance of an arbitrary particle. *Journal of Fluid Mechanics* **12**, 35–48 (1962).
- [21] Davis, A. Slow viscous flow due to motion of an annular disk; pressure-driven extrusion through an annular hole in a wall. *Journal of Fluid Mechanics* **231**, 51–71 (1991).
- [22] Trahan, J. F., Hussey, R. & Roger, R. The velocity of a circular disk moving edgewise in quasi-steady stokes flow toward a plane boundary. *Physics of Fluids* **11**, 2463–2470 (1999).

- [23] Trahan, J. F. Stokes drag on a thin circular disk moving edgewise midway between parallel plane boundaries (2006).
- [24] de Gennes, P. G. *Soft interfaces: the 1994 Dirac memorial lecture* (Cambridge University Press, 2005).
- [25] De Gennes, P.-G. & Gennes, P.-G. *Scaling concepts in polymer physics* (Cornell university press, 1979).
- [26] Landau, L. & Levich, B. *Physicochim. Acta. Physicochim (URSS)* **17**, 42 (1942).
- [27] Derhaguin, B. *Physicochim. Acta. Physicochim (URSS)* **20**, 349 (1943).